Powder Technology 272 (2015) 34-44

Stability of stainless-steel nanoparticle and water mixtures

You Young Song[a], H. K. D. H. Bhadeshia[a,b], Dong-Woo Suh[a,*]

[a]*Graduate Institute of Ferrous Technology, POSTECH, Republic of Korea*

[b]*Materials Science and Metallurgy, University of Cambridge, UK*

Abstract

Fluids containing particles that are small enough to remain in suspension over prolonged periods of time sometimes exhibit exceptional thermal properties. While considerable work has been reported on such mixtures based on oxides, inert powders and non-corrosive fluids, the present work explores the stability and thermal conductivity of mixtures of fine particles of stainless steel and pure water. In particular, aspects of sedimentation and the ability to obtain dispersals of particles with the fluid and avoid agglomeration were studied. Amongst the parameters studied, it is found that controlling the hydrogen ion concentration helps to stabilise the mixtures more than the addition of surfactants in case of 0.017 wt% stainless steel-water fluids. This is important in obtaining ζ-potentials that are large enough to sustain a significant repulsion between like particles in the fluid. The work forms the foundation of future studies on the properties of such mixtures, especially for heavy metallic particles. For 0.017 wt% stainless steel-distilled water nanoparticle-fluid, the thermal conductivity increases by 8.3 % at the optimal stability condition of *pH* 11.

Keywords: Stainless steel, Nanofluid, Stability, Thermal conductivity, pH, Surfactant

1. Introduction

Fluids containing dispersions of particles have been known for some time to have enhanced properties such as heat conduction [1] and there has been considerable modern work on fluids containing extremely small particles, on the scale of a few nanometres [2–8]. The particles studied range from oxides to intermetallic compounds, metals (Cu,Fe) and carbon nanotubes [9–16]. Attention has been focused on the ability of these particle-containing fluids to conduct heat away more rapidly than the fluid alone, both in bulk heat-transfer experiments and when the fluids are present in tiny channels [17–19].

Thermal conductivity enhancement has been reported to be higher when metallic nanoparticles are dispersed in the fluid than in the case for oxides [7, 20]. However, rapid thermal conductivity degradation, enhancement of over 20 % decreasing to almost 0 % within 30 min, was also observed for copper dispersed in water

*Corresponding author
Email address: dongwoo1@postech.ac.kr (Dong-Woo Suh)
Phone number: +82-54-279-9030 (office), +82-54-279-9299 (fax)

[21]. In addition, due to oxidation, storage and safety problems and difficulties in production because of larger particle density related to metallic particles, metallic nanoparticle-fluids have been studied much less than oxides or nanotube dispersions.

An important characteristic of a nanoparticle-fluid mixture or nanofluid is its stability with respect to the agglomeration and sedimentation of the minute particles. Previous studies have shown the particle dispersion stability can be increased by controlling *pH* of fluids or adding surfactants, and the thermal conductivity of nanofluids were higher with better stability [12, 22–28].

It may also be necessary to avoid gross chemical reactions between the particles and the fluid. For example, rusting, so in the case of the pure iron particles the fluid involved was ethylene glycol [14], whilst copper particles were dispersed into water [12] and ethylene glycol [29–31].

Besides the metallic powder was studied previously, stainless steel nanopowder may be a potential candidate because of the resistance to corrosion or chemical reaction with fluid. Also, to benefit the higher heat transfer properties of metallic-nanofluids, there is a need to study their stability first.

The purpose of the present curiosity-driven work was to see whether a suspension of stainless steel nanoparticles in water could be made stable and how much it can improve the heat conduction. Although the thermal conductivity of stainless steel itself is much lower than copper, if thermal conductivities of produced stable stainless steel-water fluids show comparable thermal conductivity enhancement to that of copper, it will show the importance of achieving stability. The work is challenging because the dynamic viscosity of water is an order of magnitude smaller than that of ethylene glycol at 20 °C [32] and the smallest nanoparticles of stainless steel that could be obtained are about 70 nm in size, much larger than the 10 nm iron particles previously studied [14].

2. Experimental

2.1. Material

Stainless steel 316L nanopowder manufactured by RND Korea to purity or 99.9 % with 70 nm mean diameter was used in this study. Fig. 1 is a transmission electron microscope (JEOL, JEM-2100) image of the particles; spherical shaped and measured average particle size is 67 ± 20 nm. The chemical composition of nanoparticles analysed by using inductively coupled plasma spectrometer (SHIMADZU, ICPE-9000) is listed in Table 1. Compared with the typical specification of 316L [33], analysed carbon content was 0.057 wt% which exceeds the maximum carbon content of 316L stainless steel.

Distilled water was used for base fluid in this work, and the detailed properties such as density, dielectric constant, refractive index and thermal conductivity of particles and water are listed in Table 2. To control the *pH* value of the base fluid, hydrochloric acid (HCl) or sodium hydroxide (NaOH) were added to distilled water (*pH* 7.04 at 20 °C). *pH* was measured with a precise pH meter of 0.01 resolution (HANNA Instruments, HI 8424). Sodium dodecyl sulphate (SDS) from Samchun Chemical Korea, sodium dodecyl benzene sulphonate (SDBS) from Sigma Aldrich, and hexadecyltrimethyl-ammonium bromide (CTAB) from Sigma Aldrich, were tested as the surfactants.

2.2. Stability Measurement

To compare the degree of stability and durability of nanoparticle-fluids, five different methods were used: sedimentation observation, transmission electron microscope (TEM) observation, particle size distribution measurement, zeta potential measurement and absorbance measurement. Sedimentation was observed to examine the durability by comparing the change of color thickness visually over time. A drop of nanoparticle-fluid on a carbon-coated copper grid (Ted Pella, CA) was dried for over 24 hours and then the effect of *pH* or surfactant on particles were observed with TEM. The stability of particles suspended in a fluid was studied by measuring the size distribution and zeta potential with Zetasizer (Malvern Instruments, Nano-ZS) within an hour and absorbance with UV/Vis scanning spectrophotometer (Beckman Coulter, DU 730) over time at rest. Previous study showed both zeta potential and absorbance are especially important in finding stable suspension conditions [12].

There are two big limitations on determining the particle size distribution using dynamic light scattering: (1) since the size is calculated by the measured diffusion coefficient over time using the Stokes-Einstein equation [34], the sample should be dilute enough for the light to be scattered and (2) non-spherical or aggregated particles cannot be distinguished as the given diffusion coefficient from the equipment is the averaged hydrodynamic diameter that is regarded to be equivalent to one sphere which has the identical diffusion coefficient. In addition, the calculated size is the hydrodynamic diameter, a sum of the particle diameter and the Debye length κ^{-1}, thus always larger than the real particle size. The Debye length is the thickness of the diffuse layer, ions that surround the surface to the slipping plane and moves with the particle within the fluid. Therefore, with the aid of the measured hydrodynamic particle size distribution, the dispersion status and the breakdown of particle aggregates can be compared.

The zeta potential ζ is the surface charge at the 'slipping plane', based on the electrophoresis theory. A larger $|\zeta|$ indicates stronger surface charge, stronger ion boundary surrounding the charged particle, and smaller κ^{-1}. The total interparticle potential between particles can be calculated by Derjaguin, Landau, Verwey and Overbeek (DLVO) theory [35, 36], and the measured zeta potential is used to calculate the repulsion force between two particles. This zeta potential can be increased by controlling the *pH* of the fluid. The suspension must be sufficiently transparent to determine the ζ potential and the particle size distribution. Also, because both measurements assume that the colloid is stable during measurement, the given data will not be reliable if sedimentation occurs rapidly.

Absorbance of a colloid at a given wavelength, A, is a measure of how much the particles in the fluid absorb light: if the particles dispersed in the fluid are not dissolved and stay in a well-dispersed state, they will absorb energy and light will scatter when exposed to a beam of light. By Beer-Lambert law, absorbance is a function of the particle concentration c [37]: $A = \epsilon bc$, where ϵ is the molar absorptivity of the particle and b is the path length of the sample, 1 cm in this study. When the sedimentation of particles occurs, the concentration of upper part will decrease and absorbance will decrease. Thus, if the absorbance is measured repeatedly over time under identical conditions, the concentration change of a sample due to sedimentation can be evaluated by the absorbance change as $c(t)/c(0) = A(t)/A(0)$ where t is time after production and $A(0)$ and $c(0)$ are the initial absorbance and concentration, respectively. In addition, absorbance measurement is applicable for lower to higher concentrations than particle size distribution or zeta potential measurements, therefore useful in estimating stability of various nanofluids at various concentrations.

2.3. Nanoparticle-fluid Production

To produce a nanoparticle-fluid with particular mass fraction, the exact amount of particles and fluid were placed in the solution-container, a 50 ml conical tube with a 28 mm diameter and 115 mm height. Agitation was done by immersing the solution-container in a bath subjected to ultrasonic pulses at 40 kHz to improve the dispersion of particles; this is the two-step method, a standard practice in the production of nanofluids [23]. The sonication temperature and time, *pH* of fluid and surfactant type and concentration were varied in order to characterise the optimum conditions.

To find the optimal stability conditions for stainless steel-water fluids, first the sonication temperature were determined to $23-25\,^{\circ}$C. To measure ζ potential and particle size distribution, the particle concentration was reduced from 1 wt% until the ζ measurements became reliable at 0.017 wt%, yielding a ζ potential of 20 mV with little deviation. This concentration was therefore chosen to further investigate the roles of *pH* and surfactant additions. The size of production was fixed to 50 ml, the sonication time to 1 h, and then the optimal *pH* of fluid that forms electrostatic stabilisation was found.

To control the *pH* of the base fluid, NaOH was added to fresh distilled water to prepare fluids with *pH* of 8.0, 9.0, 10.0, 11.0 and 12.6 at $20\,^{\circ}$C. Since HCl dissolves stainless steel, base fluid with $pH < 7.0$ was abandoned. After sonication, the ζ-potential and absorbance over time were measured. At *pH* values where stable ζ-potentials and higher absorbance could be recorded, SDS, SDBS and CTAB surfactants were added to enhance the dispersion stability. SDBS was found to achieve better stability, so this was further characterised by varying concentrations until the best stability was found.

2.4. Transient Hot-wire Method

Thermal conductivity of fluids was measured using transient hot-wire method to study the relationship with stability. Principles, apparatus design and corrections on transient hot-wire method are well documented in [38–45]. The apparatus in Fig. 2a consists of Agilent E3620A DC power supply, two fixed resistors, an adjustable resistor, a thermal conductivity cell with platinum wire, National Instruments cDAQ-9174 and 9205 data acquisition system and a computer to record data.

In this method, a thin metallic wire is used as both a line heat-source and a temperature sensor. Given voltage through the wire generates heat and increase the temperature of surrounding liquid, and the temperature of the wire over time can be calculated from the record of the voltage change over time.

The theoretical basis of the method is Fourier's law. With the assumption of constant thermal conductivity, no heat generation, and the infinite line source, the solution is [38]:

$$T(r,t) = -\frac{q}{4\pi k}E_i\left(-\frac{r^2}{4\alpha t}\right) = T_0 + \frac{q}{4\pi k}\left\{-0.5772 + \ln\left(\frac{4\alpha t}{r^2}\right) + \left[\left(\frac{r^2}{4\alpha t}\right) - \frac{1}{2^2}\left(\frac{r^2}{4\alpha t}\right)^2 + \cdots\right]\right\} \tag{1}$$

where r is the distance from the wire, t is time, q is the heat flux per unit length generated by the wire, $E_i(x) = -\int_x^{\infty}\frac{1}{u}\exp(-u)du$, T_0 is the initial temperature of a fluid at $t = 0$, k is thermal conductivity and α is the thermal diffusivity. If r is small enough, Eq. 1 is simplified as:

$$T(t) = T_0 + \frac{q}{4\pi k}\left\{-0.5772 + \ln\left(\frac{4\alpha}{r^2}\right) + \ln(t)\right]\right\}. \tag{2}$$

Then, the thermal conductivity of a fluid can be determined as:

$$k(T_\mathrm{r}) = \left[\frac{q}{4\pi(T(t_2) - T(t_1))}\right] \ln\left(\frac{t_2}{t_1}\right), \tag{3}$$

where $T(t)$ is the temperature at time t which can be calculated from the voltage change of the Wheatstone bridge, and T_r is the reference temperature of k defined as $T_\mathrm{r} = T_0 + \frac{1}{2}(\Delta T(t_1) + \Delta T(t_2))$.

Resistance of the platinum wire can be calculated from collected $\Delta V = V_1 - V_2$ by Ohm's law; $V_1 = \frac{R_2 V_s}{R_1+R_2}$, $V_2 = \frac{R_w V_s}{R_w+R_3}$, so $R_w = R_3\left\{\left(1 - \frac{R_2}{R_1+R_2} + \frac{\Delta V}{V_s}\right)^{-1} - 1\right\}$. Then the temperature change of the wire and surrounding fluid during measurement $\Delta T_\mathrm{id} = T(t) - T_0$ is calculated from the linear relationship between resistance and temperature:

$$R_\mathrm{w} = R_{T_0}\left[1 + \beta_1(T(t) - T_0)\right] \tag{4}$$

where R_{T_0} is the resistance of the wire at T_0 and β_1 is the temperature coefficient of resistance, $3.90 \times 10^{-3}\,\mathrm{K}^{-1}$ for platinum wire.

In this study, R_1 and R_2 were fixed to of $10\,\Omega$, and V_s was set to 0.55 V to have q of $0.3 - 0.4\,\mathrm{W\,m^{-1}}$. R_3 was adjusted to satisfy $\Delta V = 0$ without fluid in the cell, and ΔV was programmed to be recorded for 10 s with a rate of 600 Hz. The platinum wire of $50.8\,\mu$m in diameter and 60 mm in length was coated with a teflon layer of $< 1\,\mu$m in thickness and soldered tight to a copper wire and a platinum spring in the thermal conductivity cell of 3 cm in diameter and 10 cm in length. The resistance of the platinum wire used in this study is $R_w = 3.14\,\Omega$ at $T_0 = 20\,^\circ$C.

In addition, the effect of the insulation layer, finite wire properties and finite outer cell diameter discussed in [40, 41, 44] were considered, and corrections δT_i following the references were made to the measured temperature rise ΔT_id. Thus, $T(t)$ used in Eq. 3 to calculate the thermal conductivity should be $T(t) = T_0 + \Delta T_\mathrm{id} + \delta T_i$.

Thermal conductivity of distilled water at $20 - 40\,^\circ$C was measured for the reference and the estimated accuracy of the present method was ±5%, compared with data in [46] as shown in Fig. 2b.

3. Results and Discussion

3.1. Light absorption of stainless steel particles

Fig. 3a shows the UV-Vis spectra of stainless steel particles dispersed in distilled water. Because a small peak is observed at the wavelength of 330 nm in 0.017 wt% stainless steel-water fluids, absorbance at 330 nm was used afterwards in determining the sedimentation. Fig. 3b shows the linear relationship between absorbance and particle concentration follows the Beer-Lambert law. Therefore, $A(0) = 0.567$ at the wavelength of 330 nm and $c(0) = 0.017$ wt% can be used to determine the sedimentation of 0.017 wt% stainless steel-water nanoparticle fluids over time. This method was also used in [47].

3.2. Temperature Control

The sonication bath temperature had to be controlled because the temperature of water in the sonication bath increased up to 45 °C from 20 °C after an hour of sonication. The dynamic viscosity of water decreases from

1.01×10^{-3} kg m^{-1}s^{-1} at 20 °C to 6.31×10^{-4} kg m^{-1}s^{-1} at 45 °C [32]. From Stoke's law, the sedimentation velocity is a function of temperature, the primary effect being the change in the viscosity of the water; the sedimentation of particles can be slowed down by increasing the fluid viscosity [48]. To control the temperature, the water in the bath was refreshed with cold water at a sufficient rate to maintain the targeted temperature of 23 – 25 °C.

The effect of temperature control is shown by sedimentation observation in Fig. 4 and Fig. 5. For comparison, sedimentation of alumina (Al_2O_3) particles manufactured by Sigma Aldrich, having mean particle size of 13 nm and 45 nm in water were also tested. The sedimentation of stainless steel-water at ambient temperature is much slower in case of temperature controlled group A of Fig. 4, being a few days, than group B of Fig. 5 when the temperature of the bath was uncontrolled and allowed to rise. However, alumina-water fluids do not show apparent difference between group A and B, presumably because of the lower density and the smaller size of alumina compared with stainless steel particles; the calculated sedimentation rate of stainless steel particles is at least an order of magnitude faster than that of alumina particles.

The dependence of sedimentation rate of stainless steel-water fluids on temperature is shown in Fig. 6a,b in terms of particle size distribution and concentration change over time. When sonication bath temperature is not controlled, particles aggregate more easily and sedimentation occurs faster, consistent with the results in Figs. 4 and 5. These results give the importance of considering temperature on the stability, particularly in metallic nanoparticle-fluid mixtures.

3.3. Process Scale

To assess reproducibility as a function of the size of the experiment, the size of the fluid produced was increased from 15 ml to 50 ml whilst maintaining identical experimental conditions, including the duration of sonication of 1 h. The temperature of the sonication bath was controlled at 23-25 °C, and the fluids were assembled in tubes of identical length (115 mm) but different diameters (15 mm for 15 ml, 28 mm for 50 ml). The concentration of stainless steel particles in all cases was 0.017 wt% in order to facilitate sufficient transparency for distribution and potential measurements.

The resulting size distribution data presented in Fig. 7a shows that for the same sonication, the particles in the larger volume of fluid are less dispersed, having a greater possibility to aggregate and settle down. The ζ-potential plotted in Fig. 7b shows that although both are close to the stability of colloidal suspension in terms of $|\zeta| \gtrsim 30$ mV [2], the 15 ml sample has higher surface potential, probably stronger repulsion between particles and difficult to aggregate. The size of production was also increased to 1 L with identical conditions, but because the particles remained aggregated severely after 1 h sonication, it was impossible to measure the particle size distribution and ζ-potential due to fast sedimentation. Results show that the required sonication conditions for sufficient dispersion will also depend on the process scale, which has not been mentioned in most of the previous studies on nanofluids, which can explain the reason of the failure in reproducibility. Although 15 ml sample shows better stability here, the size was considered to be too small to test stability and thermal conductivity in this study. Therefore, the experiments afterwards were done in 50 ml scale to find the optimal stability condition with *pH* control and surfactant.

3.4. Sonication Time

The effect of sonication time is shown in Fig. 8 in terms of the particle size distribution and zeta potential when the sonication temperature and the process scale were controlled. While the ζ-potential does not vary

much, the particle size distribution results show that particles are well dispersed when sonication time is increased from 30 min to 60 min and then may aggregate with longer sonication of 90 min. Therefore, the sonication time of 60 min was selected in this study.

3.5. pH Effect

The 316L stainless steel contains iron, chromium, nickel, molybdenum, manganese, silicon and carbon as in Table 1. While the isoelectric points (IEP)[1] of Fe, Cr and Ni are known to be $pH > 7$ [49], values of $pH\,3-4$ have been quoted for the surface of stainless steels which are covered with oxide layers [50]; the ζ-potential of the mixture is expected to be in a stable range when the pH of the fluid is far from the IEP of the stainless steel particles.

With reference to the sodium hydroxide experiments, Fig. 9a shows the ζ-potential change with respect to the pH of 0.017 wt% nanoparticle-fluids. The charged surfaces of particles become unstable when the pH increases from 7 to about 9, and the IEP of 0.017 wt% stainless steel particles in distilled water was found to be pH 7.8. IEP of $pH > 7$ tell the surface of particles used in this study is not oxidized.

Further addition of NaOH increases the number of anions that surround the particles, leading to electrostatic stabilisation at pH 10 and pH 10.9 where ζ-potentials are -49.8 ± 0.6 mV and -59.0 ± 4.2 mV, respectively. At pH 12.6, the excess ions suppress the electrical double layer of the particles, the Debye length decreases, and the repulsive force between particles decreases; the excess OH^- ions disrupted the electrostatic stabilisation. The corresponding absorbance data in terms of $c(t)/c(0)$ are shown in Fig. 9b, measured from 20 min to 60 min after the production. All samples have identical concentrations, thus the concentration over time is greater in samples with less sedimentation. The sedimentation was slowest at pH 11, consistent with the ζ-potential results.

These experimental results were verified by the total interparticle potential V_T calculations based on DLVO theory [35, 36]. V_T is the sum of the van der Waals attraction V_A and repulsion V_R as a function of interparticle distance H [34] as:

$$\begin{aligned} V_T &= V_A(H) + V_R(H) \\ V_A &= -\frac{A_{131}}{6}\left[\frac{2{r_p}^2}{H^2 + 4r_pH} + \frac{2{r_p}^2}{H^2 + 4r_pH + 4{r_p}^2} + \ln\left(\frac{H^2 + 4r_pH}{H^2 + 4r_pH + 4{r_p}^2}\right)\right] \\ V_R &= 2\pi\varepsilon_m\varepsilon_0 r_p\zeta^2 \exp(-\kappa H). \end{aligned} \tag{5}$$

where r_p is the particle radius, ε_m is the static dielectric constant of medium, and ε_0 is the vacuum permittivity 8.85×10^{-12} C^2 J^{-1} m^{-1}. The interaction constant of particle 1 in medium 3, A_{131}, is Hamaker constant or Lifshitz-van der Waals constant [51–55]:

$$A_{131} = \frac{3}{4}k_BT\left(\frac{\varepsilon_p - \varepsilon_m}{\varepsilon_p + \varepsilon_m}\right)^2 + \frac{3\hbar\nu_e}{16\sqrt{2}}\frac{\left({n_p}^2 - {n_m}^2\right)^2}{\left({n_p}^2 + {n_m}^2\right)^{3/2}}, \tag{6}$$

where ε_p is the static dielectric constant of the particle and n_p and n_m are the refractive indices of the

[1]The isoelectric point (IEP) is a pH when the electrophoretic mobility is zero and the point of zero charge (PZC) is a pH when the net charge of the surface of the particle is zero. Generally, IEP and PZC can be used interchangeably.

particle and the medium. k_B is the Boltzmann constant 1.38×10^{-23} J K^{-1}, T is the absolute temperature of the medium, $\hbar$ is the Dirac's constant 1.05×10^{-34} J s and ν_e is the frequency where the dielectric medium has the strongest absorption peak, 3.0×10^{15} s^{-1} for water [55, 56].

To be consistent with the zeta potential measurement, the refractive index of stainless steel 316L at the wavelength of 633 nm was selected. The dielectric constant was calculated from the relation with refractive index as $\varepsilon = n^2$ in the static field [53]. Then the Liftshitz-van der Waals constant of stainless steel particles in water was calculated to be $A_{131} = 2.88 \times 10^{-19}$ J, which is in the range of $2 \times 10^{-19} - 5 \times 10^{-19}$ J known for metals [55]. The value of parameters used in the calculation are listed in Table 2.

The Debye length κ^{-1} [nm] of a particle in medium can be calculated as [12, 55]:

$$\kappa^{-1} = \sqrt{\frac{\varepsilon_m \varepsilon_0 k_B T}{2 N_A e^2 I}} = 1.9878 \times 10^{-3} \sqrt{\frac{\varepsilon_m T}{I}}, \tag{7}$$

where N_A is the Avogadro constant 6.022×10^{23} mol^{-1} and e is the charge of a proton 1.602×10^{-19} C. $I = \frac{1}{2} \sum_{i=1}^{n} c_i {z_i}^2$ is the ionic strength of the fluid in the unit of [mol L^{-1}] or [M] where c_i is the molar concentration of ion i [mol L^{-1}] and z_i is the charge number of ion i. In 1:1 electrolyte water whose pH value is dependent on HCl or NaOH without any salts, the Debye length is a function of the ionic concentration of H^+ or OH^-. At 300 K:

$$\kappa^{-1} = 0.3083 \sqrt{I^{-1}} \qquad \begin{cases} I = 10^{-pH} & (pH < 7) \\ I = 10^{-14+pH} & (pH > 7). \end{cases} \tag{8}$$

Therefore, the total interparticle potential of stainless steel particles in water can be calculated using the measured ζ-potential as shown in Fig. 10. The primary maximum at pH 10 and pH 11 is over $50\, k_B T$, higher than the maximum energy of the Brownian collision [48, 55], so the particles will be electrostatically stable. Since the attractive force is independent of pH of the fluid, the positive energy barrier formed for pH 10 and pH 11 are because of the strong repulsive potentials between particles with higher absolute ζ-potentials. Therefore, the dependence of the stability on interparticle forces can be explained by this calculation with ζ-potential measurement.

For the 0.017 wt% STS-water nanoparticle-fluids produced in this study, the optimal pH found is pH 11 which shows good stability without any surfactant addition. In addition, Fig. 9 and Fig. 10 show that zeta potential and sedimentation by absorbance measurements should be considered together to determine the overall stability of nanoparticle-fluids.

3.6. Surfactant Effect

In previous studies, the optimal surfactant concentration has been found only at optimal pH values [12, 24, 25]. However, the excess addition of any ions can lower the dispersoid stability. Therefore, the surfactant effect was characterised also for other samples with lower pH in this study because the addition of surfactants at the optimal pH 11 may accelerate aggregation of particles due to high concentration of ions.

First, to establish the type of the surfactant best suited for the stainless steel nanoparticle-water fluid, anionic SDS and SDBS and cationic CTAB were added to 0.017 wt%-water fluids at pH 7. Fig. 11a,b show the result of SDBS and CTAB addition, where the mass fraction of SDBS and CTAB relative to stainless steel particles

was varied as 0.5, 1.0 and 1.5. In case of SDS, the addition to fluid greatly increased the sedimentation rate, and it was impossible to measure the potential.

The addition of anionic SDBS changed the sign of ζ-potential; the particle surface is thus surrounded by adsorbed anions. Both SDBS and CTAB addition increased $|\zeta|$ – the anionic or cationic "heads" of the surfactant molecules are adsorbed to the particle surface and confer steric stability. Results show that the decrease in particle concentration is slowest when SDBS and CTAB to particle mass ratio is 0.5 and 1.0 (SDBS 0.5 and CTAB 1.0), respectively.

However, CTAB was not tested more for several reasons: sedimentation was slower when SDBS was added; it is preferable to add as little surfactant as possible to investigate the heat transfer mechanism between metallic nanoparticles, so adding SDBS with mass ratio of 0.5 is better; cationic surfactants is known not to work well in high *pH* solutions; and it is easier to use surfactants that do not change the sign of the previously formed ion boundary, thus anionic type is preferable in NaOH added fluids. Therefore, SDBS was selected on the basis of steric stabilisation.

The effect of SDBS addition at various *pH* is shown in Fig. 12 by ζ-potential change. The addition of SDBS was very effective in distilled water (*pH* 7) but not significant at NaOH added samples, especially at *pH* 10 – *pH* 11 where the electrostatic stabilisation was previously formed. ζ-potential decreases at some *pH* when SDBS is added more to the fluid; SDBS 0.5 is sufficient to from steric stabilisation and there will be excessive ions in SDBS 1.0 and SDBS 1.7 fluids. At *pH* 7, the anionic heads adsorbed to the particle surfaces easily and formed steric stabilisation since no other salts or NaOH had been added before.

The sedimentation results in Fig. 13a,b,c also show that SDBS 0.5 is the optimal condition. As the concentration of SDBS increases, decrease in $c(t)/c(0)$ increases, which implies an *increase* in sedimentation rate. This is because excessive surfactants increase both the ions adsorbed on the particle surface and the remaining counter ions. The latter will enter into the inner adsorbed layer, leading to a decrease in the ζ-potential of the particle, and hence to a decreased interparticle repulsion. Therefore from the ζ-potential and absorbance measurements, the optimal SDBS mass fraction relative to stainless steel nanoparticles is 0.5 for *pH* controlled 0.017 wt% stainless steel-water mixtures.

3.7. Optimal Conditions and Long Term Stability

The ζ-potential and long term stability of the 0.017 wt% nanoparticle-fluids with the better stability are compared in Fig. 14 and Fig. 15 for the optimal conditions found in previous sections. The $|\zeta|$ of the SDBS 0.5 fluids are slightly higher than *pH* 10 and *pH* 11 fluids, but the sedimentation is slowest at *pH* 11 fluid until 150 min. Fig. 15a shows particles settle down rapidly for 3 h and only less than 20 % of particles remain dispersed in the fluid. After 3 h, sedimentation rate is relatively slower and the overall long term stability was 10 days for *pH* 11, 3 days for *pH* 10 and DW, and less than 1 day for other fluids.

Before concluding that NaOH or SDBS addition help stainless steel particles dispersion, there is a need to identify that no chemical reaction take place between additives and particles. After storing fluids at stay for 5 days after production, the particle morphology was observed by TEM. Fig. 16 shows there is no apparent particle shape change compared with Fig. 1, so using NaOH or SDBS is thought not to cause any chemical reaction.

Above results show the electrostatic stabilisation is more effective in conferring greater stability than steric stabilisation for the 0.017 wt% stainless steel-distilled water nanoparticle-fluids. It can be concluded that

pH 11 is the optimal stability condition found for 0.017 wt% stainless steel-water nanoparticle-fluids having slowest sedimentation rate.

3.8. Thermal conductivity at optimal conditions

Fig. 17 shows the thermal conductivity enhancement, k_{nf}/k_f that is measured for the samples in Fig. 14 at 24 – 26 °C. To measure the thermal conductivity using the conductivity cell in Fig. 2a, 250 ml of sample is required. Because the process scale was fixed to 50 ml in previous stability investigations, several identical fluids were prepared at once and mixed before the thermal conductivity measurement for consistency.

Fig. 17a shows that the measured thermal conductivity enhancement is higher when the overall stability is better; measured k_{nf}/k_f at 10 min after production is highest at *pH* 11 sample, the most stable fluid among studied. Large deviations and k_{nf}/k_f ranging under 1.0 having smaller k_{nf} than water, is probably because of rapid sedimentation during measurements. Although the time of the measurement is very short, particles will continuously settle down as shown in Fig. 15.

Fig. 17b presents the thermal conductivity enhancement as a function of particle concentration for *pH* 11 fluids. It shows that the thermal conductivity enhancement increases as particle concentration increases. Thermal conductivity enhancement of 8.3 % with very small amount of stainless steel particles of 0.0021 vol.% is significant, far exceeding the Maxwell's prediction [1]. This is comparable to the 23.8 % enhancement with 0.1 vol.% copper particles in water reported [21].

However, the decrease of thermal conductivity enhancement was too fast, converging to 1.0 in 30 min. Although 30 min is longer than 10 min reported for copper-water fluids [21], there is a need to slow down the sedimentation to make use of excellent initial heat transfer property of stainless steel-water fluids.

4. Conclusions

The stability (resistance to sedimentation) of stainless steel nanoparticles and water mixtures has been characterised, including the tendency of the particles to avoid agglomeration. The parameters studied include size distribution, ζ-potential and absorbance change of the nanoparticles in distilled water with *pH* control and surfactant additions. It is clear that both ζ-potential and absorbance (sedimentation) measurements are important in measuring the stability of nanoparticle-fluids.

Dispersion via ultrasonic vibration was used to induce the separation of agglomerated particles; however, it was found that stainless steel-water mixtures require a constant low temperature in the sonication bath. Otherwise, the viscosity of the water is reduced when the temperature increases, causing rapid sedimentation during the sonication treatment. In addition, it is shown that increasing the sonication time does not always increase the stability of mixtures.

Sodium hydroxide additions were used to control the *pH* of the fluid; the isoelectric point was found to be at *pH* 7.8 for 0.017 wt% stainless steel-water mixture. The experiments revealed that *pH* 11 led to optimal condition, where the magnitude of the ζ-potential was much larger than the value of 25 mV considered as a threshold in maintaining particle separation.

The stability at *pH* 11 counter to expectations, decreased when the surfactant sodium dodecyl benzene sulphonate (SDBS) was added whereas the stability of distilled water fluid (*pH* 7) was found to increase

when the SDBS concentration was kept to about half that of the stainless steel powder. Although, the most stable condition was at *pH* 11 (*pH* 10.9 – *pH* 11.1) without any SDBS in this work. However, one of optimal conditions may have higher stability when more powerful dispersion methods are used effectively.

The long term stability was 10 days at *pH* 11, 3 days at *pH* 10 and distilled water without any addition and less than 5 hours for others. Particles settled down rapidly for 1 h after the production and the remaining dispersed particles were less than half of the initial concentration. This initial rapid sedimentation problem should be solved in the future. In addition, the reaction between particles and surfactants or *pH* controlled fluids should be considered carefully for the long term usage of fluids. No chemical reaction between NaOH and SDBS with stainless steel particles was verified.

The thermal conductivity of 0.017 wt% stainless steel nanoparticle-water fluids was higher at optimal condition, *pH* 11, showing a strong relationship between the fluid stability and heat transfer property. Thermal conductivity was increased 8.3 % at *pH* 11 fluid with 0.0021 vol.% of stainless steel particles.

Acknowledgments: Authors would like to thank Yeonggyeong Baek and Professor Sungjee Kim for assistance on zeta potential measurements. We are also grateful to Professor Kyoo Young Kim for provision of using facilities.

References

[1] J. C. Maxwell. *A treatise on electricity and magnetism*, volume 1. Clarendon Press, Oxford, U. K., 1873.
[2] S. K. Das, S. U. S. Choi, W. Yu, and T. Pradeep. *Nanofluids: Science and Technology*. John Wiley & Sons, Inc., Hoboken, New Jersey, USA, 2007.
[3] R. Saidur, K.Y. Leong, and H.a. Mohammad. A review on applications and challenges of nanofluids. *Renewable and Sustainable Energy Reviews*, 15(3):1646–1668, 2011.
[4] Y. Li, J. Zhou, S. Tung, E. Schneider, and S. Xi. A review on development of nanofluid preparation and characterization. *Powder Technology*, 196(2):89–101, 2009.
[5] D. Wen, G. Lin, S. Vafaei, and K. Zhang. Review of nanofluids for heat transfer applications. *Particuology*, 7(2):141–150, 2009.
[6] K. V. Wong and O. De Leon. Applications of Nanofluids: Current and Future. *Advances in Mechanical Engineering*, 2010:1–11, 2010.
[7] E. E. S. Michaelides. *Nanofluidics*. Springer International Publishing, Switzerland, 2014.
[8] Z. Haddad, C. Abid, H. F. Oztop, and A. Mataoui. A review on how the researchers prepare their nanofluids. *International Journal of Thermal Sciences*, 76:168–189, 2014.
[9] G. A. Longo and C. Zilio. Experimental Measurements of Thermophysical Properties of Al2O3- and TiO2-Ethylene Glycol Nanofluids. *International Journal of Thermophysics*, 34(7):1288–1307, 2013.
[10] E. V. Timofeeva, M. R. Moravek, and D. Singh. Improving the heat transfer efficiency of synthetic oil with silica nanoparticles. *Journal of Colloid and Interface Science*, 364(1):71–9, 2011.
[11] B. T. Branson, P. S. Beauchamp, J. C. Beam, C. M. Lukehart, and J. L. Davidson. Nanodiamond Nanofluids for Enhanced Thermal Conductivity. *ACS Nano*, 7(4):3183–3189, 2013.
[12] X. Li, D. Zhu, and X. Wang. Evaluation on dispersion behavior of the aqueous copper nano-suspensions. *Journal of Colloid and Interface Science*, 310(2):456–63, 2007.
[13] W. Yu, H. Xie, L. Chen, and Y. Li. Investigation on the thermal transport properties of ethylene glycol-based nanofluids containing copper nanoparticles. *Powder Technology*, 197(3):218–221, 2010.
[14] T. Hong, H. Yang, and C. J. Choi. Study of the enhanced thermal conductivity of Fe nanofluids. *Journal of Applied Physics*, 97(6):064311, 2005.
[15] L. Jiang, L. Gao, and J. Sun. Production of aqueous colloidal dispersions of carbon nanotubes. *Journal of Colloid and Interface Science*, 260(1):89–94, 2003.
[16] H. Chen, Y. Ding, and A. Lapkin. Rheological behaviour of nanofluids containing tube/rod-like nanoparticles. *Powder Technology*, 194(1-2):132–141, 2009.
[17] R. Chein and J. Chuang. Experimental microchannel heat sink performance studies using nanofluids. *International Journal of Thermal Sciences*, 46(1):57–66, 2007.
[18] L. Wang and X. Wei. Heat conduction in nanofluids. *Chaos, Solitons & Fractals*, 39(5):2211–2215, 2009.

[19] J. Fan and Y. Liu. Heat transfer in fractal channel network of wool fibre. *Materials Science and Technology*, 26(11):1320–1322, 2010.

[20] J. Fan and L. Wang. Review of Heat Conduction in Nanofluids. *Journal of Heat Transfer*, 133(4):040801, 2011.

[21] M. Liu, M. C. Lin, C.Y. Tsai, and C. Wang. Enhancement of thermal conductivity with Cu for nanofluids using chemical reduction method. *International Journal of Heat and Mass Transfer*, 49:3028–3033, 2006.

[22] Y. Hwang, J. K. Lee, Y. M. Jeong, S. I. Cheong, Y. C. Ahn, and S. H. Kim. Production and dispersion stability of nanoparticles in nanofluids. *Powder Technology*, 186(2):145–153, 2008.

[23] W. Yu and H. Xie. A Review on Nanofluids: Preparation, Stability Mechanisms, and Applications. *Journal of Nanomaterials*, 2012:1–48, 2012.

[24] X. Wang, D. Zhu, and S. Yang. Investigation of pH and SDBS on enhancement of thermal conductivity in nanofluids. *Chemical Physics Letters*, 470(1-3):107–111, 2009.

[25] X. F. Li, D. S. Zhu, X. J. Wang, N. Wang, J. W. Gao, and H. Li. Thermal conductivity enhancement dependent *pH* and chemical surfactant for Cu-H_2O nanofluids. *Thermochimica Acta*, 469:98–103, 2008.

[26] J. Philip and P. D. Shima. Thermal properties of nanofluids. *Advances in Colloid and Interface Science*, 183-184:30–45, 2012.

[27] S. Witharana, I. Palabiyik, Z. Musina, and Y. Ding. Stability of glycol nanofluids – The theory and experiment. *Powder Technology*, 239:72–77, 2013.

[28] J. Lee, K. Han, and J. Koo. A novel method to evaluate dispersion stability of nanofluids. *International Journal of Heat and Mass Transfer*, 70:421–429, March 2014.

[29] J. A. Eastman, S. U. S. Choi, S. Li, W. Yu, and L. J. Thompson. Anomalously increased effective thermal conductivities of ethylene glycol-based nanofluids containing copper nanoparticles. *Applied Physics Letters*, 78(6):718, 2001.

[30] H. Zhu, C. Zhang, S. Liu, Y. Tang, and Y. Yin. Effects of nanoparticle clustering and alignment on thermal conductivities of Fe3O4 aqueous nanofluids. *Applied Physics Letters*, 89(2):023123, 2006.

[31] J. Garg, B. Poudel, M. Chiesa, J. B. Gordon, J. J. Ma, J. B. Wang, Z. F. Ren, Y. T. Kang, H. Ohtani, J. Nanda, G. H. McKinley, and G. Chen. Enhanced thermal conductivity and viscosity of copper nanoparticles in ethylene glycol nanofluid. *Journal of Applied Physics*, 103(7):074301, 2008.

[32] Yıldız Bayazıtoğlu and M Necati Özışık. *Elements of heat transfer*. McGraw-Hill, USA, 1988.

[33] H. K. D. H. Bhadeshia and R. Honeycombe. *Steels: Microstructure and Properties: Microstructure and Properties*. Butterworth-Heinemann, 2011.

[34] William B Russel, Dudley Albert Saville, and William Raymond Schowalter. *Colloidal dispersions*. Cambridge University Press, Cambridge, U. K., 1992.

[35] B. V. Derjaguin and L. D. Landau. The theory of stability of highly charged lyophobic sols and coalescence of highly charged particles in electrolyte solutions. *Journal of Experimental and Theoretical Physics (Russ.)*, 11:802–821, 1941.

[36] E. J. W. Verwey and J. Th G. Overbeek. Theory of the stability of lyophobic colloids. *Journal of Colloid Science*, 10:224–225, 1955.

[37] D. F. Swinehart. The beer-lambert law. *Journal of Chemical Education*, 39(7):333, 1962.

[38] H. S. Carslaw and J. C. Jaeger. *Conduction of heat in solids*. Oxford University Press, New York, USA, 1959.

[39] J. J. De Groot, J. Kestin, and H. Sookiazian. Instrument to measure the thermal conductivity of gases. *Physica*, 75(3):454–482, 1974.

[40] J. J. Healy, J. J. De Groot, and J. Kestin. The theory of the transient hot-wire method for measuring thermal conductivity. *Physica B+C*, 82(2):392–408, 1976.

[41] Y. Nagasaka and A. Nagashima. Simultaneous measurement of the thermal conductivity and the thermal diffusivity of liquids by the transient hot-wire method. *Review of Scientific Instruments*, 52(2):229, 1981.

[42] Y. Nagasaka and A. Nagashima. Absolute measurement of the thermal conductivity of electrically conducting liquids by the transient hot-wire method. *Journal of Physics E: Scientific Instruments*, 14(12):1435, 1981.

[43] N. Kawaguchi, Y. Nagasaka, and A. Nagashima. Fully automated apparatus to measure the thermal conductivity of liquids by the transient hot-wire method. *Review of Scientific Instruments*, 56:1788–1794, 1985.

[44] J. G. Bleazard and A. S. Teja. Thermal conductivity of electrically conducting liquids by the transient hot-wire method. *Journal of Chemical and Engineering Data*, 40(4):732–737, 1995.

[45] G. Paul, M. Chopkar, I. Manna, and P. K. Das. Techniques for measuring the thermal conductivity of nanofluids: A review. *Renewable and Sustainable Energy Reviews*, 14:1913–1924, 2010.

[46] D. R. Lide. *CRC Handbook of Chemistry and Physics*. CRC press, 84 edition, 2004.

[47] S. Habibzadeh, A. Kazemi-Beydokhti, A. A. Khodadadi, Y. Mortazavi, S. Omanovic, and M. Shariat-Niassar. Stability and thermal conductivity of nanofluids of tin dioxide synthesized via microwave-induced combustion route. *Chemical Engineering Journal*, 156(2):471–478, January 2010.

[48] T. Cosgrove. *Colloid science: principles, methods and applications*. Wiley-Blackwell, 2010.

[49] G. A. Parks. The isoelectric points of solid oxides, solid hyroxides, and aqeous hydroxo complex systems. *Chemical Reviews*, 65:177–198, 1965.
[50] G. Lefèvre, L. Cerović, S. Milonjić, M. Fédoroff, J. Finne, and A. Jaubertie. Determination of isoelectric points of metals and metallic alloys by adhesion of latex particles. *Journal of Colloid and Interface Science*, 337(2):449–55, 2009.
[51] H. C. Hamaker. The London–van der Waals attraction between spherical particles. *Physica*, 4(10):1058–1072, 1937.
[52] J. Visser. On hamaker constants: A comparison between Hamaker constants and Lifshitz-van der Waals constants. *Advances in Colloid and Interface Science*, 3:331–363, 1972.
[53] L. Bergström. Hamaker constants of inorganic materials. *Advances in Colloid and Interface Science*, 70:125–169, 1997.
[54] S.M.S. Murshed, K.C. Leong, and C. Yang. A combined model for the effective thermal conductivity of nanofluids. *Applied Thermal Engineering*, 29(11-12):2477–2483, 2009.
[55] J. N. Israelachvili. *Intermolecular and surface forces*. Academic press, Massachusetts, USA, 3rd edition, 2011.
[56] J. Koo and C. Kleinstreuer. A new thermal conductivity model for nanofluids. *Journal of Nanoparticle Research*, 6(6):577–588, 2004.
[57] Anonymous. Refractive index database. http://www.filmetrics.com/refractive-index-database, accessed at 09-12-2013,, 2013.

Table 1: Composition in wt% of analysed stainless steel 316L particles used in this study compared with stainless steel 316L typical specification [33].

	Cr	Ni	Mo	Mn	Si	C	Fe
Analysed	17.1	11.0	2.0	0.98	0.49	0.057	bal.
[33]	16-18	10-14	2-4	1.5	1.00 max	0.03 max	bal.

Table 2: Properties of stainless steel 316L and water at 20 °C. Density (ρ), thermal conductivity (k), dielectric constant (ε) and refractive index (n) at specific wavelength (λ) are from [46] if not noted.

Material	ρ / kg m^{-3}	k / W m^{-1} K^{-1}	ε	n (λ / nm)
Stainless steel	7900	15	2.757 [57]	7.6 (633, calculated)
Water	998.21	0.5984	80.2	1.33211 (632.8)

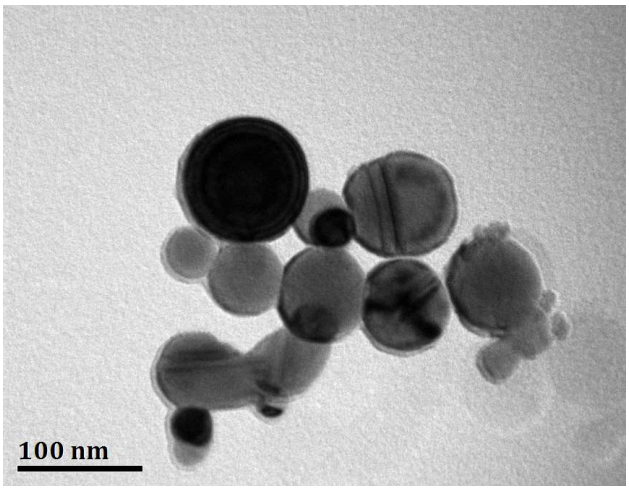

Figure 1: Bright field transmission electron microscope image of stainless steel 316L nanoparticles dispersed in distilled water. Measured average particle size is 67 ± 20 nm.

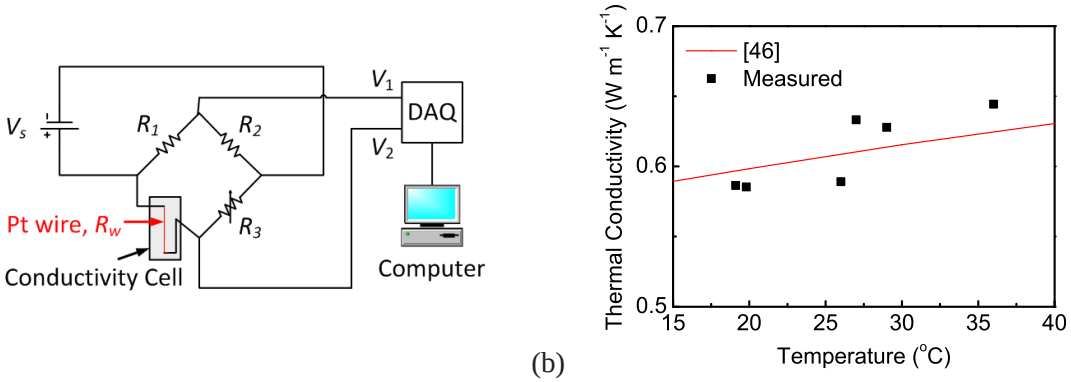

Figure 2: (a) Schematic of experimental setup of transient hot-wire circuit with thermal conductivity cell and (b) measured thermal conductivity of distilled water compared with [46].

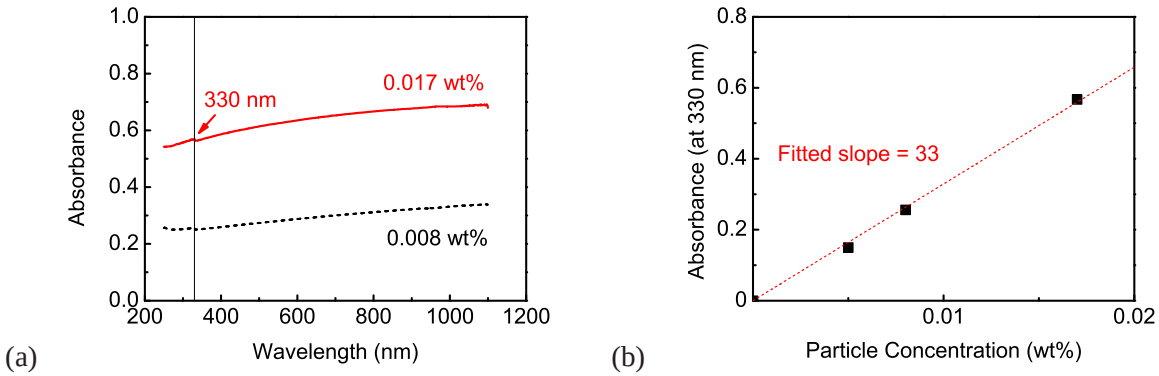

Figure 3: (a) The UV-Vis spectra and (b) relationship between particle concentration and absorbance of stainless steel 316L particles dispersed in distilled water.

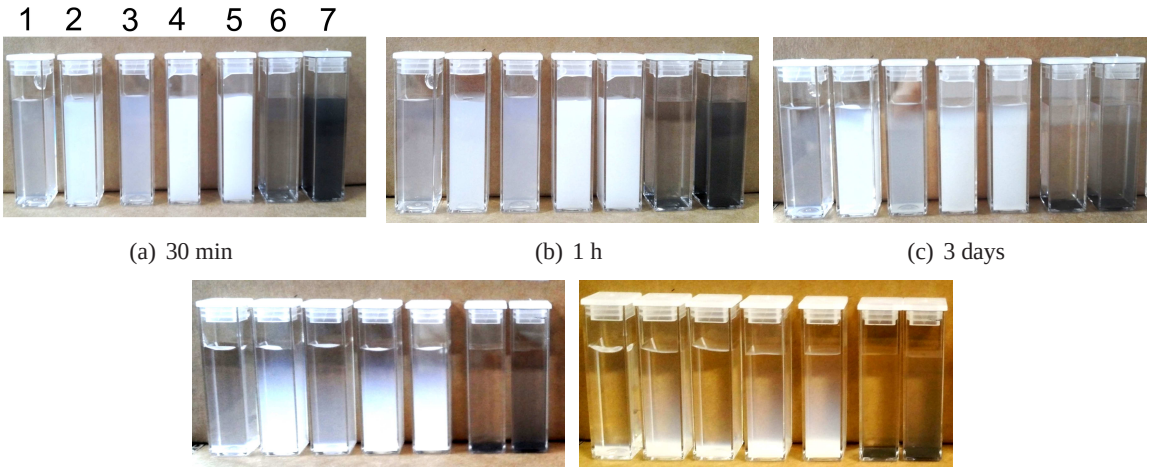

(a) 30 min (b) 1 h (c) 3 days

(d) 2 weeks (e) 1 month

Figure 4: Group A, with sonication bath temperature maintained in the range of 23 – 25 °C for 1 h. Sedimentation of water-based Al_2O_3 and stainless steel fluids as a function of time after production at rest. (1) 13 nm alumina, 0.04 wt%; (2) 13 nm alumina, 0.4 wt%; (3) 45 nm alumina, 0.04 wt%; (4) 45 nm alumina, 0.4 wt%; (5) 45 nm alumina, 0.65 wt%; (6) 70 nm steel, 0.005 wt%; (7) 70 nm steel, 0.04 wt%.

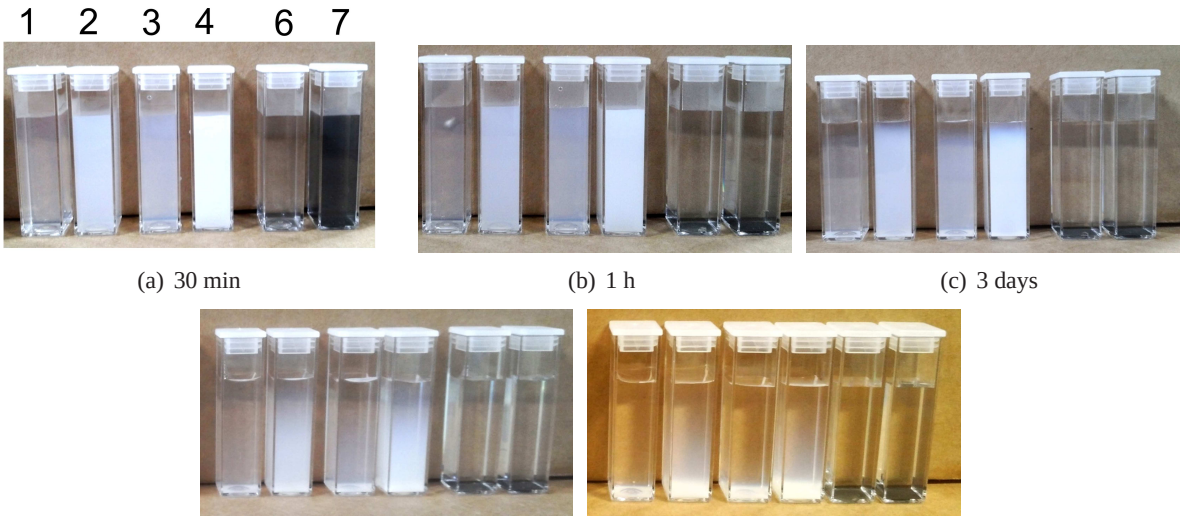

(a) 30 min (b) 1 h (c) 3 days

(d) 2 weeks (e) 1 month

Figure 5: Group B, with sonication bath temperature in the range of 23 – 45 °C for 1 h. Sedimentation of water-based Al_2O_3 and stainless steel fluids as a function of time after production at rest. (1) 13 nm alumina, 0.04 wt%; (2) 13 nm alumina, 0.4 wt%; (3) 45 nm alumina, 0.04 wt%; (4) 45 nm alumina, 0.4 wt%; (6) 70 nm steel, 0.005 wt%; (7) 70 nm steel, 0.04 wt%.

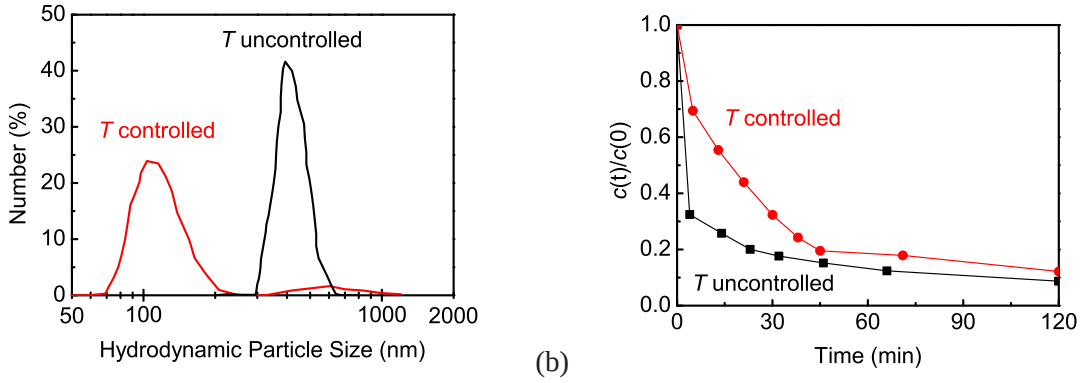

(a) (b)

Figure 6: The effect of sonication bath temperature control compared by (a) particle size distribution and (b) concentration change over time of 0.017 wt% STS - water nanoparticle-fluids. Samples were prepared using 50 ml conical tubes and were sonicated for 1 h. Measurements done within 10 min after the production.

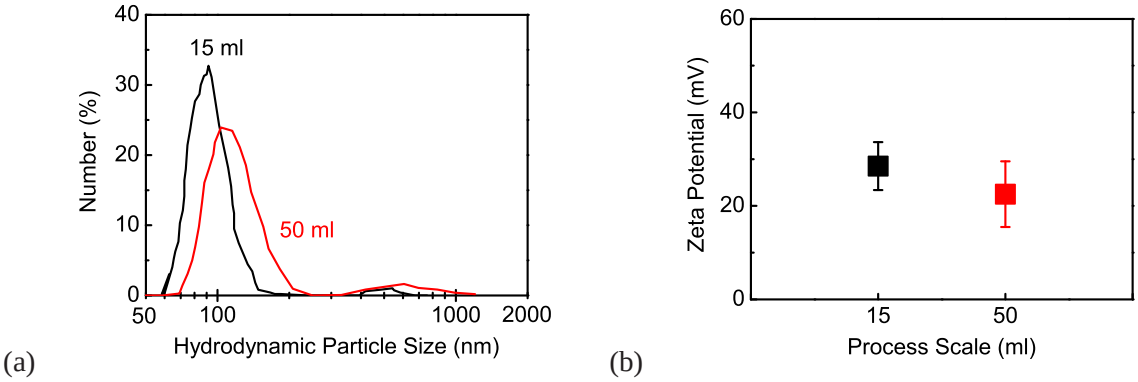

Figure 7: The effect of process scale compared by (a) particle size distribution and (b) ζ potential of 0.017 wt% STS - water nanoparticle-fluids prepared using 15 ml and 50 ml conical tubes. Measurements done within 10 min after the production.

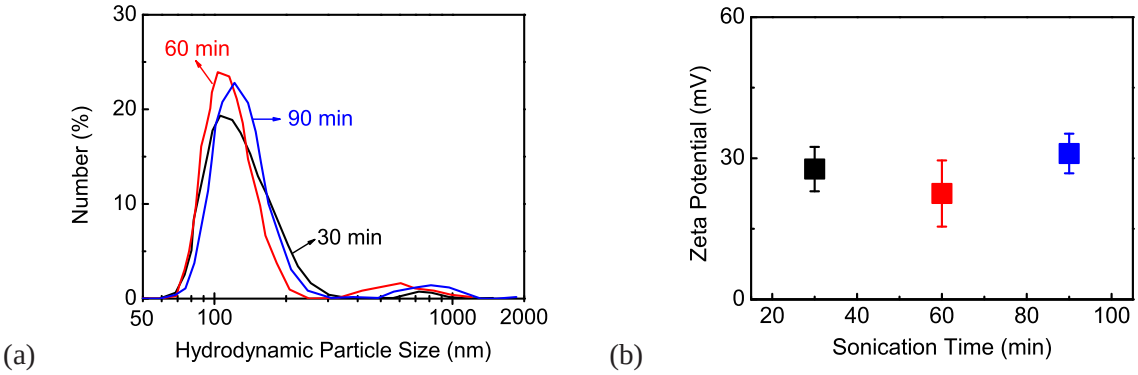

Figure 8: The effect of sonication time shown by (a) particle size distribution and (b) ζ potential of 0.017 wt% STS - water nanoparticle-fluids. Sonication temperature was controlled and the process scale was 50 ml. Measurements done within 10 min after the production.

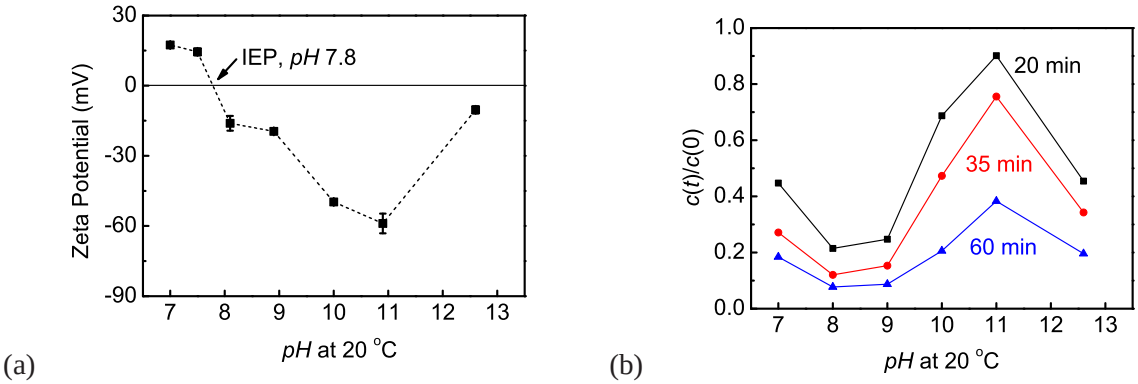

Figure 9: Measurements for 0.017 wt% stainless steel-water nanoparticle-fluids with temperature control and 1 h sonication. (a) ζ-potential as a function of *pH* varied by adding NaOH and (b) corresponding absorbance results 20 to 60 min after production represented in concentration change.

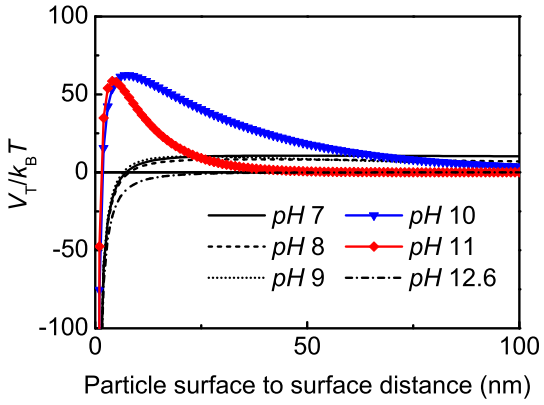

Figure 10: Calculated total interparticle potential of 0.017 wt% stainless steel-water nanoparticle-fluids in Fig. 9. $A_{131} = 2.88 \times 10^{-19}$ J, measured ζ potential from Fig. 9, calculated Debye lengths by Eq. 8, $r_p = 35$ nm and $T = 300$ K were used in calculation. The calculated Debye length at *pH* 10 and *pH* 11 are 30.8 nm and 9.75 nm, respectively.

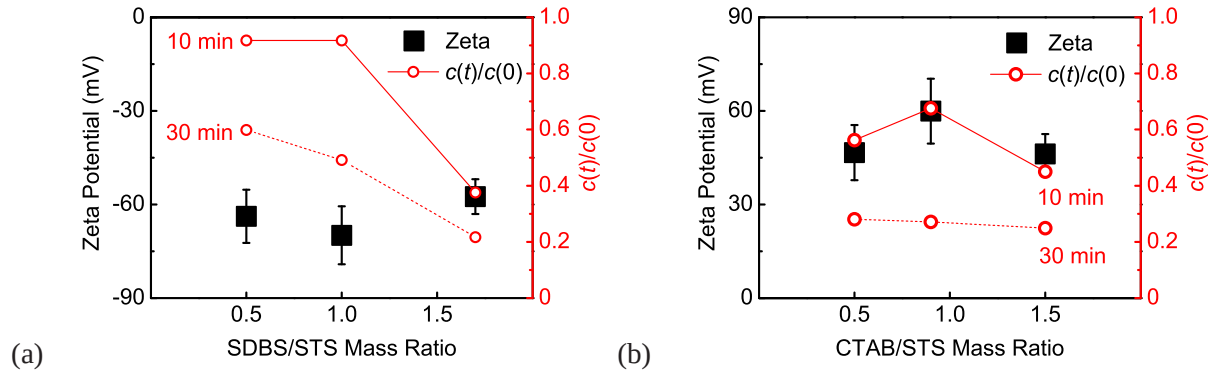

Figure 11: Effect of (a) anionic SDBS and (b) cationic CTAB surfactants on 0.017 wt% stainless steel-water nanoparticle-fluids.

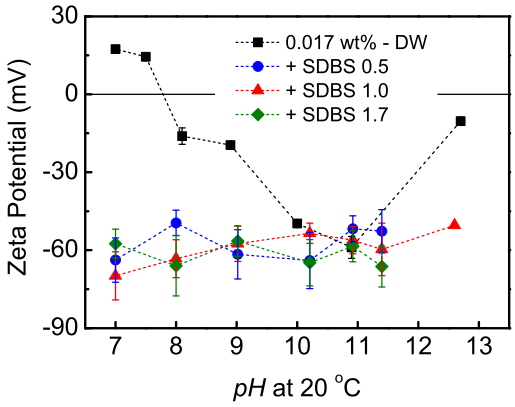

Figure 12: Effect of SDBS on the ζ potential of 0.017 wt% stainless steel-water nanoparticle-fluids with temperature controlled 1 h sonication. The mass ratios of added SDBS to stainless steel particles were 0.5, 1.0 and 1.7.

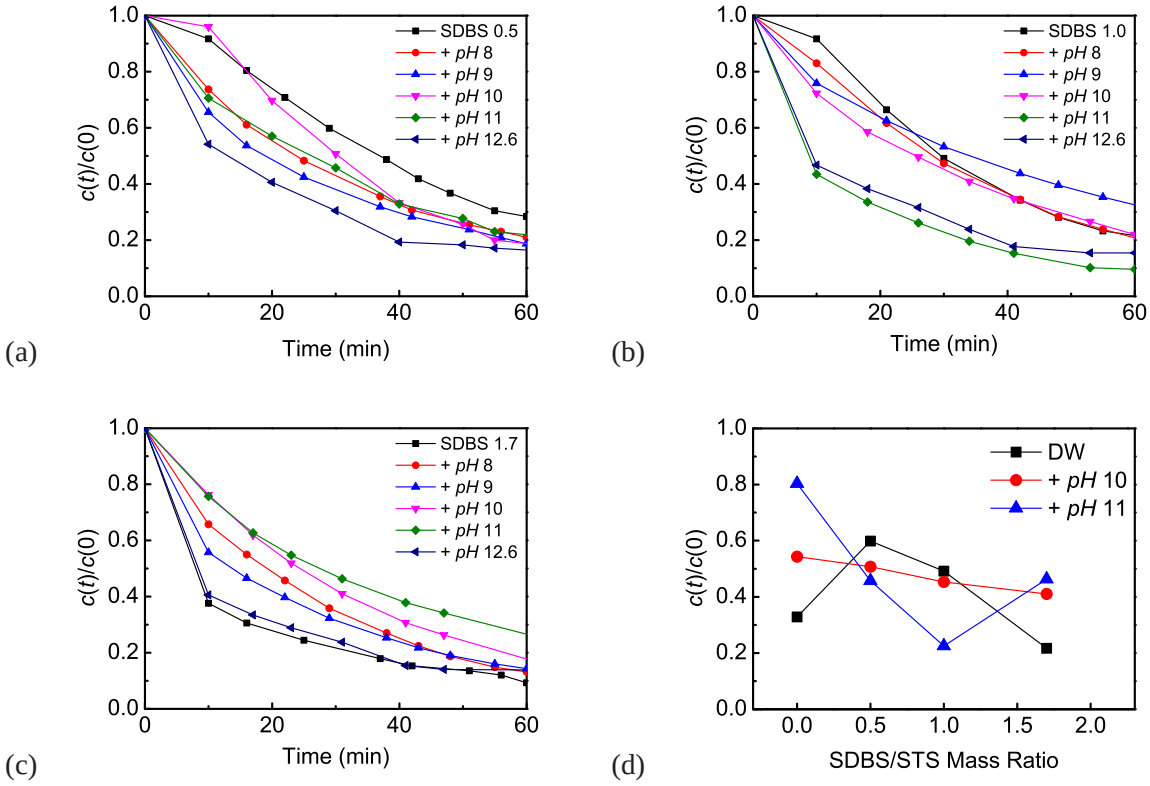

Figure 13: (a,b,c) Effect of SDBS on concentration change of fluids in Fig. 12 during 1 h. (d) Effect of SDBS concentration on stability of DW (*pH* 7), *pH* 10 and *pH* 11 fluids 30 min after production.

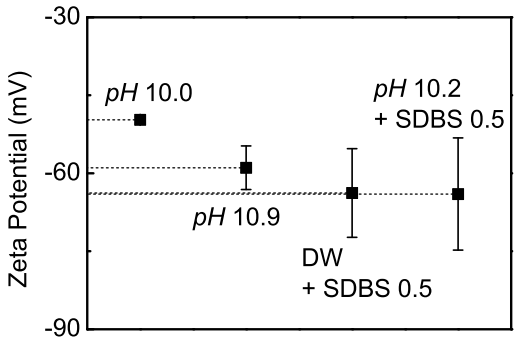

Figure 14: The ζ-potential of selected 0.017 wt% stainless steel-water nanoparticle-fluids.

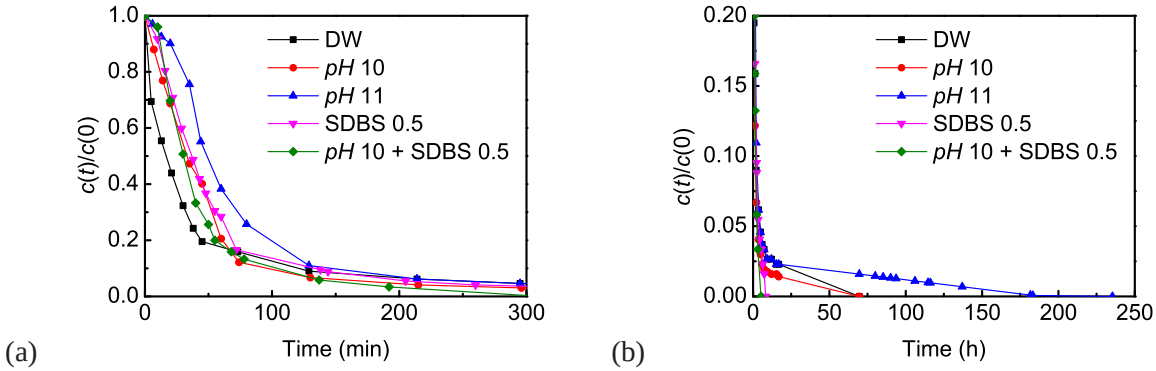

Figure 15: (a) The short term and (b) long term stability of selected 0.017 wt% stainless steel-water nanoparticle-fluids.

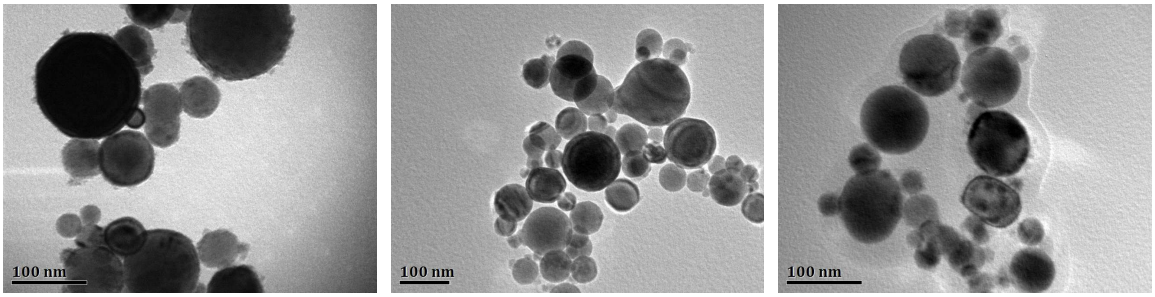

(a) pH 11 (b) SDBS 0.5 (c) pH 10 + SDBS 0.5

Figure 16: TEM images of stainless steel 316L nanoparticles dispersed in NaOH or surfactant added distilled water. To observe the effect of NaOH or surfactant on particle shape, nanoparticle-fluids were stored at stay for 5 days and then sonicated for 30 min before making the TEM sample.

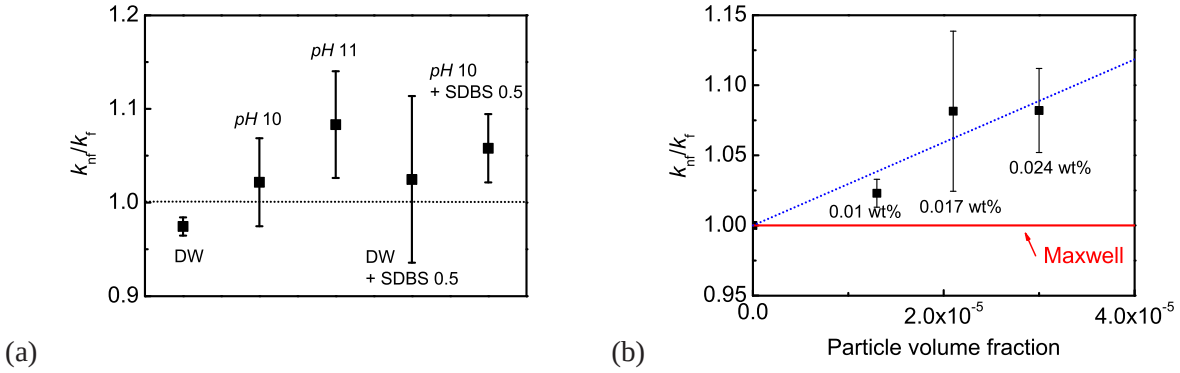

Figure 17: The thermal conductivity enhancement k_{nf}/k_f of (a) selected 0.017 wt% stainless steel-water nanoparticle-fluids and (b) *pH* 11 stainless steel-water fluids as a function of particle volume fraction. Measurement was done within 10 min after production for five to ten times.